Non-linear Optimization-Based Temperature Estimation of IPMSM

Le Sun,
Member, *IEEE*,
Nanjing University of Science and Technology
200 Xiaolingwei St.
Nanjing, 210094
sunle@njust.edu.cn

Sumedh Dhale,
Student Member, IEEE,
McMaster University
1280 Main Street West
Hamilton, ON L8S4L8, CA
dhales@mcmaster.ca

Shamsuddeen Nalakath,
Member, *IEEE*,
McMaster University
1280 Main Street West
Hamilton, ON L8S4L8, CA
nalakas@mcmaster.ca

Mustafa Mohamadian,
Member, IEEE,
FCA US LLC
1000 Chrysler Dr.
Auburn Hills, MI, USA
Mustafa.Mohamadian@fcagroup.com

Daniel Luedtke,
Member, IEEE,
FCA US LLC
1000 Chrysler Dr.
Auburn Hills, MI, USA
daniel.luedtke@fcagroup.com

Matthias Preindl,
Member, IEEE,
Columbia University
500 W. 120th Street
New York, NY 10027, USA
matthias.preindl@columbia.edu

Ali Emadi,
Member, IEEE,
McMaster University
1280 Main Street West
Hamilton, ON L8S4L8, CA
emadi@mcmaster.ca

***Abstract*—In this paper, a non-linear optimization algorithm-based temperature estimation method is presented for interior permanent magnets synchronous motor (IPMSM). Commonly the online temperature estimation scheme is realized by an abstract model with lumped-parameter thermal network. A contribution of this paper is to simplify the model by combining the thermal and loss models with essential parameters. The motor loss calibration can be avoided by this unified model. The parameters are identified by quadratic programming method. Consequently, the identified system can estimate the node temperatures online. This paper presents experimental results based on a forced-coolant IPMSM to validate the proposed method.**

Keywords— Interior permanent magnet synchronous motor (IPMSM), non-linear optimization, system identification, temperature estimation.

I. INTRODUCTION

Interior permanent magnet synchronous motor (IPMSM) is a common choice for electric vehicle powertrains. In light of this application, the installation space provided for the motor is very limited. Moreover, the desired power density of the motor is very high. Therefore, thermal loading becomes an important factor limiting the capacity of the whole drive system also affecting its reliability and endurance. Therefore, temperature limitation and management are always critical in motor drive applications [1]-[2]. For IPMSM, the most critical hotspots occur in the winding and the magnet [3]-[5].

The online temperature estimation serves as a valuable technology to manage the motor temperature [6]. For the winding, the estimation algorithm can operate along with the temperature sensor and alarms immediately for the sensor faults when the measured temperature deviates from the estimation and continue to function as an alternative to the failed sensor. On the rotor side, the sensor and slip rings can also be eliminated by estimation, [7]-[8]. Moreover, the accurate magnet temperature estimation also improves the motor control performance. For example, since the higher magnet temperature decreases PM remnant flux density, more stator current is needed to compensate the torque reduction [9]. Additionally, flux-weakening should be limited when magnets are at high temperature to avoid the risk of irreversible demagnetization [10]-[11]. Therefore, the temperature monitoring of permanent magnet is important and some of the techniques are presented in [12]-[13].

In recent years, many researchers have contributed to PM motor temperature estimation. Their proposed methods generally fall into two categories: indirect and direct estimation. Indirect methods use a motor electrical model-based observer or high frequency signal injection to calculate motor temperature sensitive parameters, e.g. winding resistance and PM flux, in order to extract the temperature information [14]-[16]. In [14] and [15], the estimation of the magnet temperature by motor and inverter electrical models is presented. The PM temperature is estimated by calculating the temperature dependent high frequency impedance under signal injection in [16]. However, the observed resistance or PM flux usually cannot accurately reflect the small temperature variations especially in applications where the noise and uncertainties have significant effect on measurements.

Direct estimation uses a motor thermal model [17]-[23]. These methods are more intuitive and effective when the precise temperature estimation is required. It is possible to model the whole motor by high fidelity lumped parameter thermal networks (LPTNs) [17]-[19]. However, for real-time implementation, the simplified thermal model is often preferred

This research was undertaken, in part, thanks to funding from the Canada Excellence Research Chairs Program, Natural Sciences and Engineering Research Council of Canada (NSERC), Automotive Partnership Canada (APC) Initiative, FCA US LLC, and FCA Canada Inc.

978-1-5386-9310-0/19/$31.00 ©2019 IEEE

[20]-[23]. Furthermore, the network parameters are identified usually by fitting the experimental data with model estimate. It is indeed a tedious and laborious method and therefore it is beneficial to use fast and simple methods to improve the modelling process.

In thermal model, the inputs are the heat sources and the outputs are the nodal temperatures. The copper, core, and magnet losses are the main heat sources [20], [23]. In [23] authors have avoided the core loss which has effect on field weakening condition. In [20], authors have set the core loss as input for the state space model. However, core loss is usually difficult to measure and calibrate accurately [24]-[25]. In some papers, the authors have used FEA or simplifying assumptions to evaluate the core loss. One issue for these papers is that they require parameter tuning work or even to measure parameter, which is unimaginable if the model has many parameters. However, for the machine in electric vehicle powertrain, even a simplified loss model needs many parameters to describe the current and frequency effect. In [18], authors have proposed a lumped-parameter method to estimate nodal temperatures and used Particle Swarm Optimization (PSO) to solve the fitting problem. Although that paper still requires measuring loss, it shows that the optimization is a good choice for thermal parameters identification and deserves further developments.

Generally speaking, the existing method usually requires empirical parameter tuning work or machine loss calibration. In this paper, a practical direct temperature estimation method is proposed. The non-linear optimization method [26]-[27] is used to solve the LPTN fitting problem. A cost function is introduced to search for a good solution of the desired parameters. The estimation model thus obtained by these parameters, can be easily embedded in real-time application. If the optimization process finds the cost function convexity to be insignificant, the trained model becomes ineffective for online temperature estimation. In terms of this issue, the training data is important to make convexity. As a practical guideline, this paper proposes a systematic method for designing the experiments to get proper training data. Eventually, a combined thermal model including a thermal network and an approximate loss model is developed. In this thermal model, core loss is not an explicit input. It is modelled as a function of flux linkage and frequency with appropriate coefficients. These coefficients are the part of input matrix (B'), and they are identified along with thermal network parameter matrix (A). Hence, it is not necessary to explicitly calibrate the core loss any more. Also, the simplification of the calculation model is discussed to improve the practicality. The experimental section discusses a common issue in real vehicular application, i.e., the estimation has to start from an uncertain initial temperature in case of the system recovering from some fault condition. The on-line temperature estimation strategy is implemented in a DSP-based real-time system and the computation amount is evaluated.

II. Thermal Model and State Space Representation

An IPMSM motor for a hybrid vehicle is investigated as an example to validate the temperature estimation strategy in this paper. The magnets on the rotor are located and arranged as V-shape layout.

A. Thermal Network with Limited Nodes

A thermal-node network is a common method to describe the motor thermal behavior. In theory, motor temperature can be estimated exactly if the number of nodes is sufficient. However, it would increase the computational effort, unsuitable for real time applications. The proposed LPTN requires only critical nodes to build an effective thermal model, viz., winding, stator core and magnet temperatures. After training the model, the LPTN model would be able to estimate the temperatures at the sensor locations. There are three assumptions taken to simplify the thermal network with the help of FEA as following.

1) Core loss is divided into three parts as stator yoke loss P_{sy}, stator teeth loss P_{sth} and rotor core loss P_r with constant split coefficients.

$$P_{sy} = k_1 P_{core},\ P_{sth} = k_2 P_{core},\ P_r = k_3 P_{core} \quad (1)$$

where k_1+k_2+k_3=1. Fig. 1 shows the FEA loss calculation result. Fig 1(a) depicts the selected calculation conditions, including maximum torque for whole speed range. Fig. 1(b) and (c) show the total core loss and the proportions between stator yoke, stator teeth and rotor core losses.

In Fig. 1 (b) and (c), the core loss increases with speed, but the proportion of rotor part (k_3) is almost a constant around 0.1. Because the flux distribution on the rotor being synchronous with the rotor rotation, the rotor core loss is always a small part of the whole core loss. On the stator side, stator yoke coefficient k_1 and stator teeth coefficient k_2 are around 0.4 and 0.5 respectively. Obviously, these two coefficients change with increasing speed, but the variation is not big.

Hence, it is reasonable to set k_1, k_2 and k_3 as constants, that helps to simplify the thermal model. However, it should be noted that the FEA analysis gives an idea that constant coefficients can be assumed, but FEA results are not used in this paper to estimate the temperature.

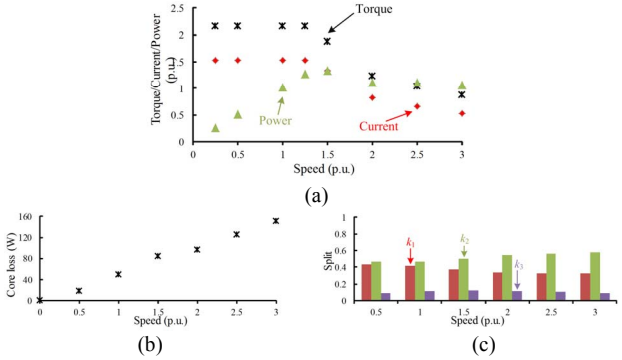

Fig. 1 FEA loss calculation. (a) Operation conditions for calculation. (b) Core Loss. (c) Split coefficients.

2) Magnet loss P_{mag} calculation is a complicated topic, especially while considering the PWM harmonics effect [28]. Yet its heating effect is not significant, as compared to the thermal conduction from stator. Hence, it is not necessary to use a precise model for real-time application. Considering equation (1), the P_r is modified to be:

$$P_r = k_3 P_{core} + P_{mag} = k_3 P_{core} + k_{m1} + k_{m2} i^2 + k_{m3} f^2 + k_{m4} i^2 f^2 \quad (2)$$

Although this assumption looks rough, it is adequate to accommodate the small heating effect on the rotor.

3) The rotor temperature sensor is installed on the magnet. The thermal conduction between magnet and rotor core is very

high, so the magnet temperature closely represents the rotor temperature. Besides, as shown in Fig. 2 (a), although the stator yoke and stator teeth are both in the stator core, their temperatures are usually different ($T_{sth} > T_{sy}$) [17].

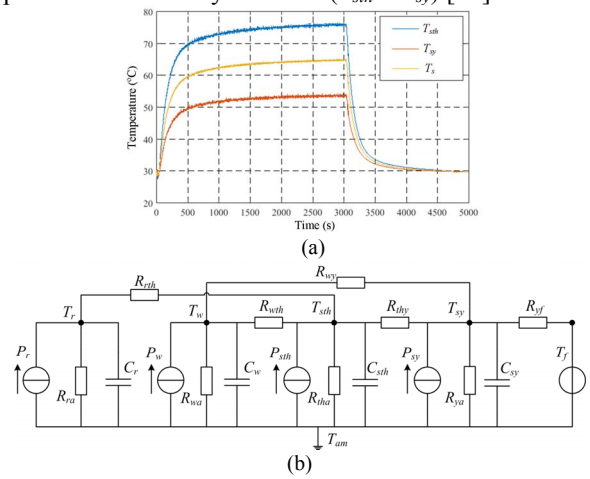

Fig. 2 Building the thermal network. (a) Temperature curves on stator teeth and yoke, and their average, operation condition: 1 per unit torque and 1 per unit speed. (b) 4-node thermal network for IPM motor.

Intuitively, the tooth temperature appears higher than yoke temperature. In Fig. 2 (a), when the T_{sth} gets 76 ˚C, the T_{sy} is only 53 ˚C. The stator tooth temperature rises mainly due to the winding copper loss and the stator yoke is close to the cooling channels. The heating of the rotor is significant when stator teeth temperature is high as the stator heat transfers to the rotor. Comparing the stator yoke and stator tooth locations, the latter is closer to the rotor and hence it is acceptable to consider only one thermal resistance between stator teeth and rotor, i.e. R_{rth}.

By the above assumption, a simplified thermal model with 4 nodes (rotor, winding and stator yoke and stator tooth) can be established in Fig. 2 (b), where P_w is copper loss in winding, P_{sth}, P_{sy} and P_r are core loss in stator teeth, stator yoke and rotor (P_r includes magnet loss) respectively. Coolant temperature T_f and ambient temperature T_{am} can be measured on the real system. For the 4 nodes, thermal capacitance of rotor C_r, winding C_w, stator teeth C_{sth} and stator yoke C_{sy} are used to emulate the thermal dynamics. Thermal resistance R_{ij} describes the heat flow between nodes, which have direct contact.

For the model in Fig. 2(b), the corresponding first-order equations describing the network dynamics are,

$$\begin{cases} \dfrac{T_r - T_{sth}}{R_{rth}} + \dfrac{T_r - T_{am}}{R_{ra}} - P_r + C_r \dfrac{dT_r}{dt} = 0 \\ \dfrac{T_w - T_{sth}}{R_{wth}} + \dfrac{T_w - T_{sy}}{R_{wy}} + \dfrac{T_w - T_{am}}{R_{wa}} - P_w + C_w \dfrac{dT_w}{dt} = 0 \\ \dfrac{T_{sth} - T_w}{R_{wth}} + \dfrac{T_{sth} - T_r}{R_{rth}} + \dfrac{T_{sth} - T_{sy}}{R_{thy}} + \dfrac{T_{sth} - T_{am}}{R_{tha}} - P_{sth} + C_{sth} \dfrac{dT_{sth}}{dt} = 0 \\ \dfrac{T_{sy} - T_{sth}}{R_{thy}} + \dfrac{T_{sy} - T_w}{R_{wy}} + \dfrac{T_{sy} - T_f}{R_{fs}} + \dfrac{T_{sy} - T_{am}}{R_{ya}} - P_{sy} + C_{sy} \dfrac{dT_{sy}}{dt} = 0 \end{cases} \quad (3)$$

the equation group (3) can be rearranged as:

$$\dot{x} = Ax + Bu \quad (4)$$

where

$$x = \begin{bmatrix} x_1 & \dots & x_4 \end{bmatrix}^T = \begin{bmatrix} T_r & T_w & T_{sth} & T_{sy} \end{bmatrix}^T,$$
$$u = \begin{bmatrix} u_1 & \dots & u_5 \end{bmatrix}^T = \begin{bmatrix} P_{core} & P_{mag} & P_w & T_{am} & T_f \end{bmatrix}^T. \quad (5)$$

The definitions of matrices A and B are listed in appendix (A1). To estimate the temperature state vector in real-time, equation (3) is transformed into discrete-time model as:

$$x(k) = x(k-1) + T_s[Ax(k-1) + Bu(k-1)] \quad (6)$$

Using (6), the current temperatures can be estimated from the previous temperatures and inputs. The temperature estimation has now been converted into two problems. The first one is to calculate the losses in vector u, and the second problem is to identify the unknown parameters in matrices *A* and *B*.

B. Loss Model

The motor losses are the heat sources in the thermal network. The copper loss P_w is usually calculated directly by Ohm's law. The only problem for such calculation is the winding resistance identification. The winding resistance magnitude R_w depends upon winding temperature and supply frequency, which are considered using following function:

$$R_w = R_{w0}[1 + \alpha_{Cu}(T_w - 20)]k_f \quad (7)$$

where α_{Cu} is a constant, defined as resistance temperature coefficient 0.004 1/K. The k_f is a coefficient employed to consider the frequency effects viz., skin and proximity effect.

$$k_f = 1 + k_{w1} f + k_{w2} f^2 \quad (8)$$

Consequently, the copper loss P_w is expressed as:

$$P_w = 1.5 R_{w0}(i_d^2 + i_q^2)[1 + \alpha_{Cu}(T_w - 20)](1 + k_{w1} f + k_{w2} f^2) \quad (9)$$

where the winding temperature is substituted by $T_w(k\text{-}1)$ in the previous sample period. Equation (9) is modified as:

$$P_w = P_{w0}(1 + k_{w1} f + k_{w2} f^2) \quad (10)$$

Unlike P_w, calculation of P_{core} is more complicated and challenging to be measured accurately. In paper [21] a temperature-dependent method is used to identify core loss on-line. The problem of this method is that the temperature sensitivity on core loss is not enough to accommodate for small variations. In paper [20], frequency and current ratios are used to calculate core loss on the basis of a rated core loss. Since this method does not consider the current phase angle and includes some nonlinear parameters which are difficult to tune it is time consuming and not very accurate.

Formula (11) is used to roughly evaluate core loss [29].

$$P_{core} = k_h B_m^2 f + k_e B_m^2 f^2 \quad (11)$$

where B_m is amplitude of the sinusoidal flux density, f is the operation frequency. The k_h and k_e are hysteresis loss and eddy current loss coefficients. The flux density is proportional to flux linkage, so equation (11) can be converted to:

$$P_{core} = k_{hd} \varphi^2 f + k_{ed} \varphi^2 f^2 \quad (12)$$

where k_{hd} and k_{ed} are coefficients analogous to those in equation (11), fusing the loss coefficients and the proportion between B_m and φ. Flux linkage φ is easy to calculate or measure at different load conditions.

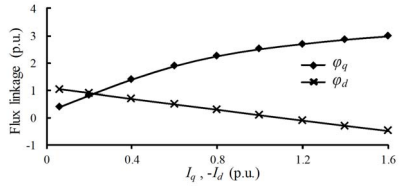

Fig. 3 Flux linkage at different load conditions. $\varphi_d(-I_d)$ and $\varphi_q(I_q)$.

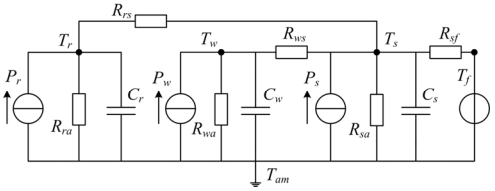

Fig. 4 Reduced 3-node thermal network.

Fig. 3 shows measured flux linkage at different load conditions. It should be noted that the q-flux linkage $\varphi_q(I_q)$ is a curve, whose slope rate reduces at heavy load. It is due to core saturation in q-axis at heavy load. The square of the net flux linkage φ^2 can be calculated as,

$$\varphi^2 = \varphi_d^2 + \varphi_q^2 \tag{13}$$

Equation (13) is an approximate formula to calculate the fundamental order core loss, yet accurate enough for temperature estimation if the coefficients can be identified well.

C. Simplified Model Combination

The coefficients k_{hd} and k_{ed} in core loss formula (12) are unknown and difficult to accurately identify from measurements. However, these coefficients can be considered as parameters of the thermal model. The input vector should be expressed only by measurable information. To achieve this, the parameters of input matrix B and input vector (5) are modified accordingly. Which leads to transformation of matrix B into B' as described in (A2) and the input vector as shown below.

$$\begin{aligned} u' = \Big[& \varphi^2 f^2 \quad \varphi^2 f \quad P_{w0} \quad P_{w0} f^2 \quad P_{w0} f \\ & i^2 \quad f^2 \quad i^2 f^2 \quad T_{am} \quad T_f \quad 1 \Big]^T \end{aligned} \tag{14}$$

In the new input vector u', φ can be estimated using the graph in Fig. 3 and equation (13), P_{w0} can be calculated from (10), T_{am} and T_f are measured inputs. Therefore, all the variables in u' can be obtained in each sample period. Furthermore, by knowing x and u, the parameters in A and B' can be identified.

D. Discuss on 3-node model

In most applications, temperature estimation precision request is not extremely high. For example, for torque compensation on temperature rise, 5°C discrepancy is acceptable. For the motor under test, the torque reduction is only 2% as T_r rises from 30°C to 70°C since the temperature-dependence of NdFeB remanent flux density is very small [30].

The winding and rotor temperatures estimations are only critical in terms of the motor protection and torque compensation. Hence, it gives a chance to consider further simplifying the LPTN proposed in the previous section. In this simplified version, the nodes T_{sth} and T_{sy} in the thermal network Fig. 2 (b) are combined to form an average node T_s, as shown in Fig. 4. Accordingly, only one stator core loss P_s is considered. The constant coefficient k_3 divides the total core loss between stator and rotor as,

$$P_r = k_3 P_{core} + P_{mag},\ P_s = (1-k_3) P_{core}. \tag{15}$$

For 3-node thermal network, a group of first-order equations are used to describe the physical behavior as,

$$\begin{cases} \dfrac{T_r - T_s}{R_{rs}} + \dfrac{T_r - T_{am}}{R_{ra}} - P_r + C_r \dfrac{dT_r}{dt} = 0 \\ \dfrac{T_w - T_s}{R_{ws}} + \dfrac{T_w - T_{am}}{R_{wa}} - P_w + C_w \dfrac{dT_w}{dt} = 0 \\ \dfrac{T_s - T_w}{R_{ws}} + \dfrac{T_s - T_r}{R_{rs}} + \dfrac{T_s - T_{am}}{R_{sa}} + \dfrac{T_s - T_f}{R_{sf}} - P_s + C_s \dfrac{dT_s}{dt} = 0 \end{cases} \tag{16}$$

which are organized as:

$$\dot{x} = A_3 x + B_3 'u' \tag{17}$$

where the state vector reduces to :

$$x = \begin{bmatrix} x_1 & x_2 & x_3 \end{bmatrix}^T = \begin{bmatrix} T_r & T_w & T_s \end{bmatrix}^T \tag{18}$$

The definitions of matrices A_3 and B_3' are listed in appendix (A3). It should be noticed that A_3 is 3 x 3, and B_3' is 3 x 11, which are smaller than A and B, that means the real-time computational burden will be lighter than the 4-nodes model.

III. Parameter Identification

A. Non-linear Optimization Based Parameters Estimation

Non-linear optimization method is used to identify the parameters in the model. Usually, a cost function is required to transform the parameter identification problem into a Non-linear optimization problem.

Initially, for a generic dynamic system such as

$$\dot{x} = f(x, u, z) \tag{19}$$

where z is vector containing all the parameters. The estimates of the parameters can be defined as:

$$\hat{z} = z - \bar{z} \tag{20}$$

where $\bar{z}$ is the estimation error. A qualifier of the estimates $\hat{z}$ can be built using a dynamic model:

$$h(\hat{z}) = f(x, u, \hat{z}) - \dot{x} \tag{21}$$

The function $h(\hat{z}) = 0$, i.e. $\| h(\hat{z}) \| = 0$ is a necessary condition for good estimation. In other words, $\hat{z} = z$, i.e. $\bar{z} = 0$ which implies $h(\hat{z}) = 0$. While the opposite is not true in general, appropriate provisions can be made such that the implication is bidirectional. In optimization-based parameter estimation, the zeros of the $h(\hat{z})$ are identified through an optimization problem

$$\hat{z}^* = \arg\min_{\hat{z} \in D} c(\hat{z}),\ c(\hat{z}) = \left\| h(\hat{z}) \right\|^2 = h(\hat{z})' h(\hat{z}) \tag{22}$$

where $c(\cdot) : D \rightarrow R$ is the cost function with search domain $D \subseteq R$. We generally assume that $h(\hat{z})$ (hence $c(\hat{z})$) is smooth, D is convex, and $z \in$ int D. By the cost function $c(\hat{z})$, the required estimation can be obtained when $c(\hat{z})$ get its minimum in the domain D such that $\hat{z}^* = z$.

B. Thermal Network Identification

In this section, the introduction of identification algorithm is presented in the context of 4-nodes model, which has 26 parameters. The algorithm is exactly same as that for 3-nodes model, which has 19 parameters. For the convenience, all the parameters in A and B are substituted by $z_1 \sim z_{26}$, the substitution is listed in appendix (table AI). Then, the equation group (4) can be rewritten as described in appendix (A4). By sorting (A4), the parameters $z_1 \sim z_{26}$ can be extracted to an exterior vector z. Then, for each sample time, a standard qualifier in (21) can be rebuilt as (23) by replacing vector z by its estimates $\hat{z}$.

$$h_1(\hat{z}) = M_1(x,u)\hat{z} + q_1 \tag{23}$$

where $\hat{z} = [\hat{z}_1 \quad \dots \quad \hat{z}_{19}]^T$, $q_1 = \dot{x}$, and $M_1(x, u)$ is defined in appendix (A5).

The M_1 (4 x 26) is constructed by data x (temperature) and u (inputs) sampled in one period. In a long time operation, all these data can be collected and serialized, resulting in a sequential database.

$$M = [M_1 \quad \dots \quad M_N]^T, q = [q_1 \quad \dots \quad q_N]^T, h = [h_1 \quad \dots \quad h_N]^T \tag{24}$$

where N is the number of sample steps.

Rewriting (23) using (24), and substituting it into (22), the cost function gets its specific form as:

$$c(\hat{z}) = h(\hat{z})' h(\hat{z}) = \hat{z}^T (M^T M)\hat{z} + [(2q^T M)\hat{z} + q^T q] \tag{25}$$

which is same as,

$$c(\hat{z}) = \hat{z}^T (H)\hat{z} + f(\hat{z}) \tag{26}$$

where $H=M^TM$ is a real symmetric matrix. Equation (26) is a standard form of a quadratic programming (QP) problem. Hence, standard QP solver is used to search for the minimum value of the cost function and to identify the desired parameters. The data matrix M has the dimensions $4N$ x 26 and the size of matrix H is 26 x 26 independent of the size of data samples.

The parameters identification depends upon the data matrix M. It should be noted that the model parameters may change in different operation points, although they are supposed to be constant in the state-space equations. This issue will be discussed in detail with experimental verification.

IV. Experiment Validation

A. 48V IPMSM Test Bench Setup

The proposed temperature estimation strategy is tested in test bench consisting of motors connected in a back-to-back setup, shown in Fig. 5. Two equal IPMSM motors are coupled together. The TI TMS320F28377D (CPU 200MHz) is used for motor controller, and a NI analog-to-digital conversion (ADC) device is used for sampling the temperatures. The sample frequency and switching frequency of the drive system are 10 kHz, which is much higher than the sample frequency of temperature sensors, 10 Hz. All the temperature information is communicated via CAN bus, so the DSP-based controller can read it in real-time and synchronize with the current and speed.

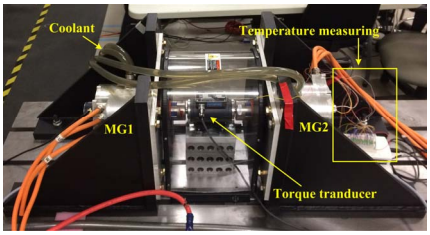

(a)

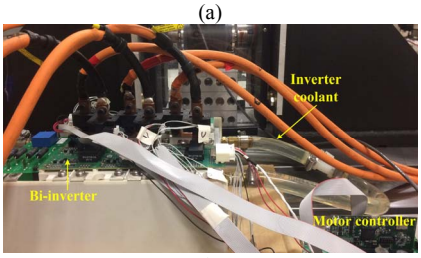

(b)

Fig. 5 IPM test bench. (a) Back-to-back motors test bench. (b) Motor drive setup (inverter and controller).

The experiment is divided into two steps. The first step is to collect experimental database for training the model. With the database, the identification algorithm in section III can identify the parameter vector z, to build the matrices A and B (or A_3, B_3). The second step consists of online temperature estimation experiment with the identified thermal model.

B. On-line Temperature Estimation

The identified parameters form the matrices A and B. With the thermal model equation; temperature estimation of (6) can be implemented in each sample step. In the real-time processor, the computation takes around 1.4 us for each step. Fig. 6(a) shows the experimental heavy load conditions for validation of the identified model (4-node). The temperature at each node is estimated and measured synchronously.

In Fig. 6(b), the estimations on all the 4 nodes are always close to measurements. Although there is some estimation error, the discrepancy between the measured and estimated temperatures is found to be less than 3°C that is an acceptable accuracy for most applications.

As compared with the 4-node model method, the only difference on the database usage is to make the average of the stator teeth and yoke. The 19 parameters can construct the matrices A_3 and B_3', which are 3 x 3 and 3 x 11 respectively. The computation time reduces to 0.9 us for each step.

Table I listed the time consumptions of the parameters identification (offline in computer before estimation) and temperature estimation (online in DSP).

TABLE I
TIME CONSUMPTIONS

Items	4-node	3-node
Parameters identification	0.65s	0.31 s
Temperature estimation	1.4 us	0.9 us

Fig. 6(c) shows the experimental validation of the identified 3-nodes model for the operating conditions in Fig. 6(a). The estimations always agree well with the measurements. The performance of 3-nodes model is as better as the 4-nodes model, with 35% less computation time in DSP. This feature is quite beneficial for low-cost applications.

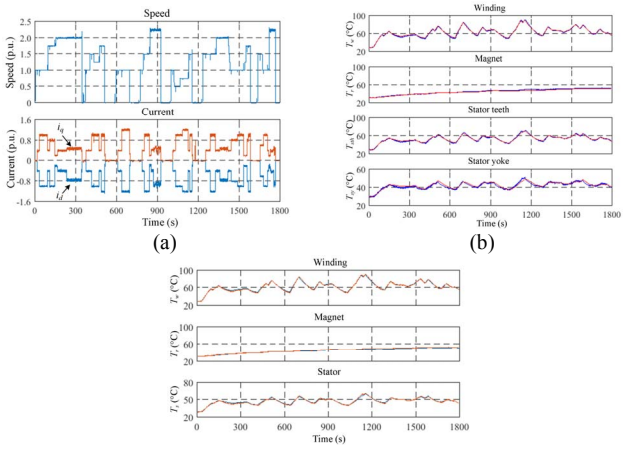

Fig. 6 Experimental validation on heavy load test. (a) Heavy load procedure. (b) Estimation by 4-node model. (c) Estimation by 3-node model. (Figure b and c, red lines: estimates, blue lines: measurement).

Similar validation is also implemented on UDDS (Urban Dynamometer Driving Schedule, Federal Test Procedure-72) drive cycle. Fig. 7 shows the test results on 4-node and 3-node models separately. In UDDS testing, the rotor temperature estimation does not perform as well as that in heavy load cycle test. Firstly, this is because the operating conditions in training database are quite similar to those of the heavy load cycle test, in which the heating is significant in comparison to the light load operation of UDDS. The estimation error is always under 3 °C, hence considered to be acceptable in this validation.

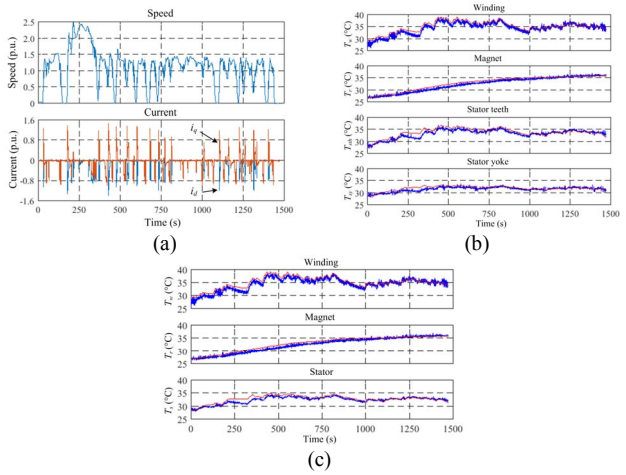

Fig. 7 Experimental validation on UDDS drive cycle. (a) UDDS procedure. (b) Estimation by 4-node model. (c) Estimation by 3-node model. (Figure b and c, red lines: estimates, blue lines: measurement).

V. Conclusion

In this paper, a simple thermal network is developed to realize online temperature estimation within 5°C error. By combining the loss model and thermal network, all the related parameters can be identified together. Such unified model identification helps to avoid the loss measurement and calibration. This is different from existing parameter identification-based method.

In contrast to some existing parameter tuning work, the thermal and loss parameters can be identified from a training database. The empirical tuning skill is not required anymore. The training database is critical to have good parameters identification. Authors investigated the influence of training data structure. Validation shows that, the proposed 4-/3-node models can perform well on temperature estimation. The 3-node model apparently has superior performance in terms of computational effort.

Additionally, a practical feature is discovered that the estimation by the proposed scheme can get convergence from uncertain initial temperature assumption, which is useful for real automotive application.

References

[1] A. Boglietti, A. Cavagnino, D. Staton, M. Shanel, M. Mueller and C. Mejuto, "Evolution and modern approaches for thermal analysis of electrical machines," *IEEE Transactions on Industrial Electronics*, vol. 56, no. 3, pp. 871-882, Mar. 2009.

[2] W. Pawlus, H. V. khang, and M. R. Hansen, "Temperature rise estimation of induction motor drives based on loadability curves to facilitate design of electric powertrains," *IEEE Transactions on Industrial Informatics*, vol. 13, no. 3, pp. 985-994, Jun. 2017.

[3] S. Stipetic, M. Kovacic, Z. Hanic, and M. Vrazic, "Measurement of excitation winding temperature on synchronous generator in rotation using infrared thermography," *IEEE Transactions on Industrial Electronics*, vol. 59, no. 5, pp. 2288–2298, May. 2012.

[4] S. Ruoho, J. Kolehmainen, J. Ikaheimo, and A. Arkkio, " Interdependence of demagnetization, loading, and temperature rise in a permanent-magnet synchronous motor," *IEEE Transactions on Magnetics*, vol. 46, no. 3, pp. 949–953, Mar. 2010.

[5] Y. Yang, B. Bilgin, M. Kasprzak, S. Nalakath, H. Sadek, M. Preindl, J. Cotton, N. Schofield and A. Emadi, "Thermal management of electric machines," *IET Electrical Systems in Transportation*, vol. 7, no. 2, pp. 104–116, Nov. 2016.

[6] Z. Lazarevic, R. Radosavljevic and P. Osmokrovic, "A novel approach for temperature estimation in squirrel-cage induction motor without sensors," *IEEE Transactions on Instrumentation and Measurement*, vol. 48, no. 3, pp. 753–757, Jun. 1999.

[7] C. Mejuto,M.Mueller,M. Shanel, A. Mebarki, M. Reekie, and D. Staton, "Improved synchronous machine thermal modelling," in *Proc. 2008 18th International Conference on Electrical Machines (ICEM'2008)*, Vilamoura, Portugal, Sep. 2008, pp. 1–6.

[8] M. Ganchev, H. Umschaden, and H. Kappeler, "Rotor temperature distribution measuring system," in *Proc. 2011 37th Annual Conference of the IEEE Industrial Electronics Society (IECON'2011)*, Melbourne, Australia, Nov. 2011, pp. 2006–2011.

[9] S. Li, B. Sarlioglu, S. Jurkovic, N. R. Patel and P. Savagian, "Comparative analysis of torque compensation control algorithms of interior permanent magnet machines for automotive applications considering the effects of temperature variation," *IEEE Transactions on Transportation Electrification*, vol. 3, no. 3, pp. 668–681, Sep. 2017.

[10] J. Hong, S. Park, D. Hyun, T. J. Kang, S. B. Lee, C. Kral, and A. Haumer, "Detection and classification of rotor demagnetization and eccentricity faults for PM synchronous motors," *IEEE Transactions on Power Electronics*, vol. 48, no. 3, pp. 923–932, May/Jun. 2012.

[11] S. Zhu, M. Cheng, W. Hua, X. Cai and M. Tong, "Finite element analysis of flux-switching pm machine considering oversaturation and irreversible demagnetization," *IEEE Transactions on Magnetics*, vol. 51, no. 11, pp. 7403404, Mar. 2015.

[12] G. Feng, C. Lai, K. Mukherjee and N. C. Kar, "Online PMSM magnet flux-linkage estimation for rotor magnet condition monitoring using measured speed harmonics," *IEEE Transactions on Industry Applications*, vol. 53, no. 3, pp. 2786 - 2794, Mar. 2017.

[13] Y. Da, X. Shi, and M. Krishnamurthy, "A new approach to fault diagnostics for permanent magnet synchronous machines using electromagnetic signature analysis," *IEEE Transactions on Power Electronics*, vol. 28, no. 8, pp. 4104– 4112, Aug. 2013.

[14] A. Specht and J. Bocker, "Observer for the rotor temperature of IPMSM," in *Proc. 2010 14th International Power Electronics and Motion Control Conference (EPE-PEMC'2010)*, Ohrid, Macedonia, Sep. 2010, pp. 1–4.

[15] O. Wallscheid, A. Specht and J. Bocker, "Observing the permanent-magnet temperature of synchronous motors based on electrical fundamental wave model quantities," *IEEE Transactions on Industrial Electronics*, vol. 64, no. 5, pp. 3921 - 3929, May. 2017.

[16] S. D. Wilson, P. Stewart, and B. P. Taylor, "Methods of resistance estimation in permanent magnet synchronous motors for real-time thermal management," *IEEE Transactions on Energy Conversion*, vol. 25, no. 3, pp. 698–707, Aug. 2010.

[17] J. Fan, C. Zhang, Z. Wang, Y. Dong, C. E. Nino, A. R. Tariq, and E. G. Strangas, "Thermal analysis of permanent magnet motor for the electric vehicle application considering driving duty cycle," *IEEE Transactions on Magnetics*, vol. 46, no. 6, pp. 2493–2496, Jun. 2010.

[18] J. Nerg, M. Rilla, and J. Pyrhonen, "Thermal analysis of radial-flux electrical machines with a high power density," *IEEE Transactions on Industrial Electronics*, vol. 55, no. 10, pp. 3543–3554, Oct. 2008.

[19] S. Zhu, M. Cheng, and X. Cai, "Direct coupling method for coupled field-circuit thermal model of electrical machines," *IEEE Transactions on Energy Conversion*, 10.1109/TEC.2017.2761787.

[20] C. Kral, A. Haumer, and S. B. Lee, "A practical thermal model for the estimation of permanent magnet and stator winding temperatures," *IEEE Transactions on Power Electronics*, vol. 29, no. 1, pp. 455–464, Jan. 2014.

[21] O. Wallscheid, and J. Bocker, "Global identification of a low-order lumped-parameter thermal network for permanent magnet synchronous motors," *IEEE Transactions on Energy Conversion*, vol. 31, no. 1, pp. 354–365, Mar. 2016.

[22] O. Wallscheid, and J. Bocker, "Fusion of direct and indirect temperature estimation techniques for permanent magnet synchronous motors," in *Proc. 2017 IEEE International Electric Machines and Drives Conference (IEMDC'2017)*, Miami, FL, May 2017, pp. 1–8.

[23] C. Sciascera, P. Giangrande, L. Papini, C. Gerada, and M. Galea, "Analytical thermal model for fast stator winding temperature prediction," *IEEE Transactions on Industrial Electronics*, vol. 64, no. 8, pp. 6116–6126, Aug. 2017.

[24] P. Handgruber, A. Stermecki, O. Biro, A. Belahcen, and E. Dlala, "Three-dimensional eddy-current analysis in steel laminations of electrical machines as a contribution for improved iron loss modeling," *IEEE Transactions on Industry Applications*, vol. 49, no. 5, pp. 2044–2052, Sep./Oct. 2013.

[25] M. Fasil, N. Mijatovic, B. B. Jensen, and J. Holboll, "Nonlinear dynamic model of pmbldc motor considering core losses," *IEEE Transactions on Industrial Electronics*, vol. 64, no. 12, pp. 9282-9290, Dec. 2017.

[26] S. Boyd, and L. Vandenberghe, *Convex Optimization*. New York, NY: Cambridge University Press, ISBN: 978-0-5218-3378-3, March 2004.

[27] G. Mercere, O. Prot, and J. A. Ramos, "Identification of parameterized gray-box state-space systems: from a black-box linear time-invariant representation to a structured one," *IEEE Transactions on Automatic Control*, vol. 59, no. 11, pp. 2873 - 2885, Nov. 2014.

[28] S. Zhu, M. Cheng, and Y. Zhu, "Fast calculation of PM eddy current loss in IPMSM under PWM VSI supply based on the spectra of line-line voltage," *IEEE Transactions on Magnetics*, early access. 2018.

[29] K. Yamazaki and Y. Seto, "Iron loss analysis of interior permanent-magnet synchronous motors-variation of main loss factors due to driving condition," *IEEE Transactions on Industry Applications*, vol. 33, no. 4, pp. 1045–1052, Jul./Aug. 2006.

[30] M. D. Calin and E. Helerea, "Temperature influence on magnetic characteristics on Nd-Fe-B permanent magnets," in *Proc. 2011 7th International Symposium on Advanced Topics in Electrical Engineering (ATEE'2011)*, Bucharest, Romania, May 2011.